Hermitian symmetry free optical-single-carrier frequency division multiple access for visible light communication

Ali Waqar Azim, Yannis Le Guennec, Ghislaine Maury

Hermitian Symmetry Free Optical-Single-Carrier Frequency Division Muliple Access for Visible Light Communication

Ali W. Azim[a,*], Yannis Le Guennec[a], Ghislaine Maury[a]

[a] *Université Grenoble Alpes, CNRS, Institute of Engineering, Grenoble INP, IMEP-LAHC, F-38000 Grenoble, France*

Abstract

Optical-orthogonal frequency division multiplexing (O-OFDM) is an effective scheme for visible light communications (VLC), offering a candid extension to multiple access (MA) scenarios, i.e., O-OFDMA. However, O-OFDMA exhibits high peak-to-average power ratio (PAPR), which exacerbates the non-linear distortions. To oust high PAPR while sustaining MA, optical-single-carrier frequency-division multiple access (O-SCFDMA) is used. For both O-OFDMA and O-SCFDMA, Hermitian symmetry (HS) constraint is imposed in the frequency-domain (FD) to obtain real-valued time-domain (TD) signal for intensity modulation-direct detection (IM-DD) implementation of VLC. Howbeit, HS constraint results in an increase of PAPR for O-SCFDMA. In this regard, we propose HS free (HSF)O-SCFDMA which averts the use of HS. We compare HSFO-SCFDMA with several approaches in key parameters, such as, bit error rate (BER), PAPR, quantization, electrical power efficiency and system complexity. Simulations are performed considering multipath VLC channel and taking into account the bandwidth limitation of light emitting diode (LED) in combination with its driver. It is illustrated that HSFO-SCFDMA outperforms other alternatives.

Keywords: Intensity modulation-direct detection, optical-orthogonal frequency division multiplexing, peak-to-average power ratio, optical-single-carrier frequency domain multiple access.

1. Introduction

Over the past couple of decades, there has been an exponential surge in the deployment of radio frequency (RF) wireless systems, which has led to RF spectral congestion. Visible light communications (VLC) is perceived as a complementary technology to overcome this looming RF spectral crisis. With onset of incoherent high power light emitting diodes (LEDs) and sensitive photo-detectors (PDs), VLC has gained a substantial interest [1]. Along with some compelling advantages, such as, license free unlimited optical bandwidth, high-security and no electromagnetic interference, VLC is appealing as it offers both lighting and communication concurrently.

*Corresponding author. Tel./fax: +33-660-380-994

Email addresses: azima@minatec.grenoble-inp.fr (Ali W. Azim), leguennec@minatec.grenoble-inp.fr (Yannis Le Guennec), ghislaine.maury@minatec.grenoble-inp.fr (Ghislaine Maury)

For VLC, optical-orthogonal frequency division multiplexing (O-OFDM) is an effective approach as it can allow high data-rates, simple one tap equalization in the frequency-domain (FD) and show inherent resilience to combat inter-symbol-interference (ISI) resulting from dispersive multi-path propagation [2–5]. In VLC, O-OFDM operates using simple, low-cost intensity modulation-direct detection (IM-DD). In IM-DD, the intensity waveform modulates onto the brightness of the LED which is photo-detected at the receiver. Thus, for IM-DD implementation, the time-domain (TD) signal is necessitated to be real-valued and non-negative. Several tailored O-OFDM schemes satisfying IM-DD constraints, such as, direct-current (DC)O-OFDM [2], asymmetrically clipped (AC)O-OFDM [3], Flip-OFDM [6], Hermitian symmetry (HS) free (HSF)-OFDM [7] etc have been proposed.

Despite advantages, one operational limitation of O-OFDM is its unavoidable high peak-to-average-power ratio (PAPR), which makes it susceptible to non-linear distortions [8, 9]. Besides, due to an increase in quantization noise, limited bit resolution of digital-to-analog converters (DACs) and analog-to-digital converters (ADCs) also bound the performance [10]. Various methods [8, 9, 11] and [12] have been devised to counteract high PAPR. Though, an increased complexity overhead and/or bandwidth inefficiency is associated with these techniques.

To realize a complete networking VLC system, multiple access (MA) is essential [13, 14]. O-OFDM provides a straightforward extension to MA, i.e., O-OFDMA, where the subcarriers are allocated to different users based on a pre-defined resource allocation matrix. However, O-OFDMA also manifests high PAPR, thus, non-linear distortions are inevitable. To surmount the distortions and to accommodate MA, optical-single carrier frequency division multiple access (O-SCFDMA) is used[1]. O-SCFDMA is a discrete Fourier transform (DFT)-precoded variant of O-OFDMA and its foremost advantage is lower PAPR [15]. In the literature, O-OFDMA inspired O-SCFDMA schemes, e.g., ACO- and DCO-SCFDMA [15] have been introduced. Both ACO- and DCO-SCFDMA manifest lower PAPR relative to O-OFDMA counterparts while satisfying HS constraint. Nevertheless, Wu *et al.* [16] have identified that in VLC merely half of the TD symbols exploit single-carrier (SC) like benefits for O-SCFDMA because of HS, whereas in RF systems, all the TD symbols act like SC. Hence, it can be deduced that if HS is enforced, DFT-precoding results in a less compelling PAPR reduction. Consequently, the precoded schemes which rule out the need of HS have shown to surpass others (which use HS) in their efficacy for PAPR reduction. Recently, SC optical frequency division multiplexing (SCO-FDM) has been investigated in [17]. SCO-FDM exhibits lower PAPR compared to ACO-OFDMA/SCFDMA, while demonstrating the same bit error rate (BER) in an additive white Gaussian noise (AWGN) channel for a given electrical signal-to-noise ratio (SNR). However, the PAPR is not reduced to mininum level as in interleaved (I)-SCFDMA for RF systems because of insertion of zeros in the TD signal [16]. Low complexity pulse-amplitude modulation (PAM) based discrete Hartley transform (DHT)-spread ACO-OFDM (DHTS-ACO-OFDM) has been proposed

[1]In the sequel, we use the terms subcarrier and subchannel for O-OFDMA and O-SCFDMA, respectively, to distinguish between the two systems.

by Zhou and Qiao [18] and [19] which also averts HS. DHTS-ACO-OFDM features lower PAPR compared to ACO-OFDMA/SCFDMA, however, with an increase in size of modulation alphabet, PAPR reduction becomes less efficient.

Against what has been reported in the literature, we propose an O-SCFDMA approach capable of attaining superior performance compared to other alternatives. The main contributions of this work are:

1. An O-SCFDMA approach, HS free (HSF)O-SCFDMA is introduced. HSFO-SCFDMA yields a number of concrete advantages over other alternatives, such as, lower PAPR, power and cost efficiency.
2. Performance of HSFO-SCFDMA has been assessed considering multipath VLC channel and bandwidth limitation of LED/LED driver combination. For comparison, together with HSFO-SCFDMA, we have adopted ACO-SCFDMA, DHTS-ACO-OFDM, SCO-FDM, and DCO-SCFDMA. We evaluate key performance parameters, such as, PAPR, BER, computational complexity, quantization, electrical power and spectral efficiency.
3. Optical power penalty due to bandwidth limitation of LED/LED driver combination and multipath VLC channel is evaluated. We demonstrate that HSFO-SCFDMA suffers the least optical power penalty.
4. We evaluate closed-form PAPR expressions as a function of modulation alphabets for the approaches which exhibit constant PAPR.

The rest of the article is organized as follows. In Section 2, we present HSFO-SCFDMA. Additionally, we provide a brief description of multipath VLC channel and bandwidth limitation of the LED/LED driver combination. In Section 3, we present a succinct analysis of the statistical characterization of HSFO-SCFDMA, where the average electrical and the average optical powers are evaluated. We provide simulation results in Section 4. In Section 5, we describe the MA for HSFO-SCFDMA. Based on obtained results, conclusions are drawn in Section 6.

1.1. Notation

Unless otherwise mentioned, lower-case boldface letters are used to denote TD symbol vectors, e.g., $\mathbf{s}$. Moreover, lower-case letters with super-scripted index, like $\mathrm{s}^{(n)}$ represents the nth sample of the TD signal. FD symbol vectors are represented by upper-case, boldface letters, e.g., $\mathbf{S}$, whereas, upper-case letters with super-scripted index, e.g., $\mathrm{S}^{(n)}$ denote the modulated symbol on nth subchannel. $\mathbf{F}_L$ and $\mathbf{F}_L^{\mathrm{H}}$, respectively, represents $L \times L$ DFT and IDFT matrices. The (n_1, n_2)th element of DFT and IDFT matrix is obtained as $\mathbf{F}_{(n_1,n_2)} = L^{-1/2} e^{-j2\pi n_1 n_2/L}$ and $\mathbf{F}^{\mathrm{H}}_{(n_1,n_2)} = L^{-1/2} e^{j2\pi n_1 n_2/L}$, respectively, where $(n_1, n_2) \in 0, 1, \cdots, L-1$, and $j^2 = -1$. Furthermore, $\mathbb{C}^L$, $\mathbb{R}^L$, and $\mathbb{R}_+^L$ represent L-order complex vector, real-valued vector, and positive real-valued vector, respectively. Furthermore, we use $E(\cdot)$, $(\cdot)^{\mathrm{H}}$, $|\cdot|$, $(\cdot)^{\mathrm{T}}$, and $\otimes$ to represent ensemble average, Hermitian conjugate, absolute, transpose and convolution operators, respectively. Whereas, $\Re[\cdot]$ and $\Im[\cdot]$ are respectively used to obtain the real and imaginary components of a vector.

2. HSFO-SCFDMA and System Model

2.1. Modulation Concept

The foremost advantage of precluding HS is the low PAPR which is accomplished because all the TD symbols enjoy SC benefits. Contrary to that, if HS is implemented for O-SCFDMA, only half of the TD symbols manifest SC like behaviour, hence, resulting in a less significant PAPR reduction, e.g., DCO-SCFDMA and ACO-SCFDMA. Moreover, it has been established for both RF [20] and VLC [16] that I-SCFDMA culminates the lowest PAPR. Hence, in HSFO-SCFDMA, we couple the technique suggested by Fatima *et al.* [7] with I -SCFDMA, to realize an O-SCFDMA approach capable of exhibiting low PAPR, whilst complying with IM-DD constraints. Furthermore, in HSFO-SCFDMA, to obtain a real-valued TD signal is straightforward because by imitating I-SCFDMA, we modulate only the even subchannels, which naturally results in a half-wave symmetric TD signal [20], from which the real and imaginary components can be separated in a forthright manner.

In the sequel, a detailed explanation on HSFO-SCFDMA is presented considering a simplified scenario (with only one user). Firstly, the transmitter of HSFO-SCFDMA is presented. Subsequently, VLC channel model and the limited bandwidth characteristics of the LED are presented. Finally, the receiver of HSFO-SCFDMA is described.

2.2. Transmitter

HSFO-SCFDMA transmitter is illustrated in Fig. 1. The incoming bit stream is parsed into $N/2$ parallel channels using a serial-to-parallel (S/P) converter. Thereafter, the bits are modulated to Gray-mapped complex M-ary quadrature-amplitude modulation (QAM) TD complex symbols resulting in a TD symbol vector, $\mathbf{s} \in \mathbb{C}^{N/2}$. Subsequently, $\mathbf{s}$, is transformed to a FD symbol vector, $\mathbf{S}$, via $N/2$-order DFT as

$$\mathbf{S} = \mathrm{DFT}\left(\mathbf{s}\right) = \mathbf{F}_{N/2} \cdot \mathbf{s} \in \mathbb{C}^{N/2}, \tag{1}$$

which essentially represents DFT-precoding. Afterwards, subchannel mapping is performed by assigning $N/2$ FD DFT-precoded symbols from $\mathbf{S}$ to the even subchannels of another N-order FD symbol vector, $\tilde{\mathbf{S}}$, where $\tilde{\mathbf{S}}$ can be explicitly given as $\tilde{\mathbf{S}} = \left[\mathrm{S}^{(0)}, 0, \mathrm{S}^{(1)}, 0, \cdots, \mathrm{S}^{(N/2-2)}, 0, \mathrm{S}^{(N/2-1)}, 0\right]^{\mathrm{T}} \in \mathbb{C}^{N}$. The subchannels in $\tilde{\mathbf{S}}$ are mapped in an interleaved manner, because it is established that interleaved subchannel mapping leads to better PAPR performance [16].

After subchannel mapping, $\tilde{\mathbf{S}}$ is transformed to a DFT-precoded TD symbol vector by applying N-order IDFT as

$$\tilde{\mathbf{s}} = \mathrm{IDFT}\left(\tilde{\mathbf{S}}\right) = \mathbf{F}_{N}^{\mathrm{H}} \cdot \tilde{\mathbf{S}} \in \mathbb{C}^{N}. \tag{2}$$

Owing to the frame structure of $\tilde{\mathbf{S}}$, $\tilde{\mathbf{s}}$ features the following properties: (P1) $\tilde{\mathbf{s}}$ is a scaled and repeated version of $\mathbf{s}$ [17, 20]. (P2) $\tilde{\mathbf{s}}$ features half-wave symmetry, i.e., $\tilde{\mathrm{s}}^{(n)} = \tilde{\mathrm{s}}^{(n+N/2)}\ \forall\ n = 0, 1, \cdots, N/2-1$ [21]. (P1) implies that the $N/2$-order FFT and N-order IFFT at the transmitter are redundant. However, we accentuate that both are imperative for (frequency division) MA (see Section 5). By exploiting (P2), the real and imaginary sub-blocks of the half-wave symmetric signal, $\tilde{\mathbf{s}}$ can be obtained as

$$\mathbf{x}_{\Re} = \Re\left[\tilde{\mathrm{s}}^{(n)}\right],\ \mathbf{x}_{\Im} = \Im\left[\tilde{\mathrm{s}}^{(n+N/2)}\right]\ \forall\ n = 0, 1, \cdots, N/2-1, \tag{3}$$

with no loss of useful information, where $\{\mathbf{x}_{\Re}, \mathbf{x}_{\Im}\} \in \mathbb{R}^{N/2}$. From (3), it can be inferred that, a M-QAM (square) constellation is split into two $\sqrt{M}$-PAM constellations.

A cyclic prefix (CP) with a length equal to the number of channel taps is affixed to both sub-blocks. For conciseness in notation, after the addition of CP, the sub-blocks are still expressed as $\mathbf{x}_{\Re}$ and $\mathbf{x}_{\Im}$. Afterwards, $\mathbf{x}_{\Re}$ and $\mathbf{x}_{\Im}$ are concatenated to obtain $\mathbf{x} = [\mathbf{x}_{\Re} \;\; \mathbf{x}_{\Im}]^{\mathrm{T}} \in \mathbb{R}^{N+2N_{\mathrm{CP}}}$, where N_{CP} is the length of CP. $\mathbf{x}$ is impinged on a DAC to obtain an analog electrical waveform, $\mathbf{x}(t)$. $\mathbf{x}(t)$ is intrinsically bipolar, so, a bias, $\beta_{\mathrm{dc}} > 0$, is introduced, such that

$$\mathbf{x}_{\beta}(t) = \mathbf{x}(t) + \beta_{\mathrm{dc}} \in \mathbb{R}_{+}, \tag{4}$$

where $\mathbf{x}_{\beta}(t)$ is the biased HSFO-SCFDMA signal, which is transmitted through an optical channel by LED. β_{dc} is prescribed as

$$\beta_{\mathrm{dc}} = \alpha\sqrt{E[\mathbf{x}^2(t)]}, \quad \alpha > 0, \tag{5}$$

with bias-index on a decibel (dB) scale defined as $10\log_{10}(\alpha^2 + 1)$ dB. We follow *sufficient* biasing [2] for HSFO-SCFDMA, where α is adjusted, such that β_{dc} is equal to the absolute value of the negative peak of $\mathbf{x}(t)$.

In what follows, we assume perfect synchronization [8, 9, 22]. A linear response of the LED is considered in system evaluation [8, 9, 22], since, nonlinearity of the LED can be mitigated using digital pre-distortion [23].

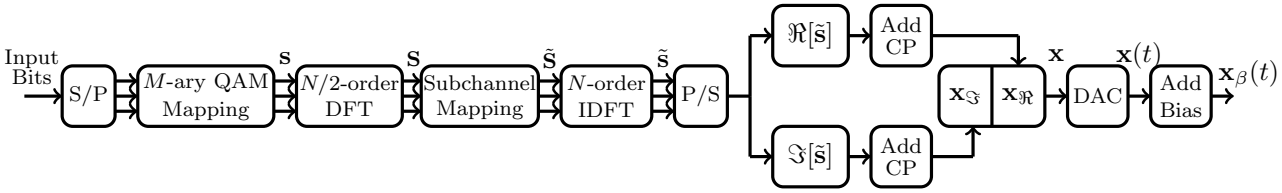

Figure 1: Block diagram of HSFO-SCFDMA transmitter.

2.3. Channel Modeling

The bandwidth limitation of the LED/LED driver combination with an impulse response $h_{\mathrm{LED}}(t)$ is modeled as a Gaussian low-pass filter with an 3 dB optical cut-off frequency, $f_{3\mathrm{dB}}$, having a transfer function of [24]

$$H_{\mathrm{LED}}(f) = e^{-\ln(2)\left(\frac{f}{f_{3\mathrm{dB}}}\right)^2}. \tag{6}$$

So, even if an ideal channel exists between the LED and the PD, the received signal would be a filtered version of the transmitted signal. Additionally, the dispersive attributes of the VLC channel can be taken into account by considering indoor environments, where the received optical signal endures time dispersion from the objects inside the room. If the indoor fixtures of the room are deemed purely diffusive, the reflections from different objects are also diffusive in nature and can be adequately modeled as Lambertian [25]. The VLC channel response would consist of both the

line-of-sight (LOS) and reflected diffuse components. Herewith, we obtain the multipath channel coefficients, $h_{\text{chan}}(t)$, using the ray tracing recursive algorithm for the indoor VLC studied by Lee *et al.* [26].

The overall channel impulse response culminating the impact of bandwidth limitation of the LED/LED driver combination and VLC channel can be given as

$$h(t) = h_{\text{LED}}(t) \otimes h_{\text{chan}}(t). \tag{7}$$

Sampling time (T_{s}) of 1 ns and up to 4 diffused reflections are considered. We consider that the transmitter and the receiver are perfectly synchronized, such that the channel is tapped from the time of arrival of LOS signal [27]. Readers are directed to [26] for a detailed analysis on channel modeling.

2.4. Receiver

The receiver of HSFO-SCFDMA is illustrated in Fig. 2. At the receiver, the light intensity is photodetected using a PD, and the bias is eliminated using a DC blocking capacitor. The received intensity waveforms, $\mathbf{y}(t)$ is electronically amplified using a transimpedance amplifier (TIA), and then fed to an ADC to yield $\mathbf{y} = [\mathbf{y}_{\Re} \;\; \mathbf{y}_{\Im}]^{\text{T}}$. The TD symbol vectors corresponding to the received real and imaginary sub-blocks after CP removal and S/P conversion are

$$\begin{aligned} \mathbf{y}_{\Re} &= \mathbf{H}\mathbf{x}_{\Re} + \mathbf{w}_{\Re} \in \mathbb{R}^{N/2}, \\ \mathbf{y}_{\Im} &= \mathbf{H}\mathbf{x}_{\Im} + \mathbf{w}_{\Im} \in \mathbb{R}^{N/2}, \end{aligned} \tag{8}$$

respectively, where, $\mathbf{w}_{\Re}$ and $\mathbf{w}_{\Im}$ can be approximately modeled as AWGN. $\mathbf{H}$ is $N/2 \times N/2$ circulant convolution matrix with the first column equal to $\mathbf{h} = [h_0, h_1, \cdots, h_{L-1}, 0, \cdots, 0]$ for L channel coefficients and $h_n = h(nT_{\text{s}})$ with $n \in [0, L-1]$. We assume a stationary VLC channel, i.e., $\mathbf{H} = \mathbf{H}_{\Re} = \mathbf{H}_{\Im}$. Furthermore, the circulant nature of $\mathbf{H}$, allows to diagonalize it using the DFT matrix and write

$$\mathbf{H} = \mathbf{F}_{N/2}^{\text{H}} \mathbf{\Lambda}_{N/2} \mathbf{F}_{N/2}, \tag{9}$$

where $\mathbf{\Lambda}$ is a diagonal matrix with the channel frequency response on its diagonal and having eigen values $\left[\Lambda_0, \Lambda_1, \cdots, \Lambda_{N/2}\right]^{\text{T}} = \mathbf{F}_{N/2}\mathbf{h}$.

The sub-blocks, $\mathbf{y}_{\Re}$ and $\mathbf{y}_{\Im}$, are transformed to FD by $N/2$-order DFT to yield

$$\begin{aligned} \mathbf{Y}_{\Re} &= \text{DFT}\left(\mathbf{y}_{\Re}\right) = \mathbf{F}_{N/2} \cdot \mathbf{y}_{\Re} \in \mathbb{C}^{N/2}, \\ \mathbf{Y}_{\Im} &= \text{DFT}\left(\mathbf{y}_{\Im}\right) = \mathbf{F}_{N/2} \cdot \mathbf{y}_{\Im} \in \mathbb{C}^{N/2}. \end{aligned} \tag{10}$$

A FD minimum mean squared error (MMSE) equalizer with the knowledge of channel impulse

response is applied to $\mathbf{Y}_{\Re}$ and $\mathbf{Y}_{\Im}$ to yield equalized FD sub-blocks as

$$\begin{aligned}\tilde{\mathbf{Y}}_{\Re} &= \left(\mathbf{\Lambda}^{\mathrm{H}}\mathbf{\Lambda} + (E_{\mathrm{b}_{(\mathrm{elec})}}/N_0)^{-1}\mathbf{I}\right)\mathbf{\Lambda}^{\mathrm{H}}\mathbf{Y}_{\Re} \in \mathbb{C}^{N/2},\\ \tilde{\mathbf{Y}}_{\Im} &= \left(\mathbf{\Lambda}^{\mathrm{H}}\mathbf{\Lambda} + (E_{\mathrm{b}_{(\mathrm{elec})}}/N_0)^{-1}\mathbf{I}\right)\mathbf{\Lambda}^{\mathrm{H}}\mathbf{Y}_{\Im} \in \mathbb{C}^{N/2},\end{aligned} \tag{11}$$

where $E_{\mathrm{b}_{(\mathrm{elec})}}/N_0$ is the electrical SNR per bit, and $\mathbf{I}$ denotes the identity matrix. Afterwards, $\tilde{\mathbf{Y}}_{\Re}$ and $\tilde{\mathbf{Y}}_{\Im}$ are transformed to TD counterparts by using $N/2$-order IDFT as

$$\begin{aligned}\tilde{\mathbf{y}}_{\Re} &= \mathrm{IDFT}\left(\tilde{\mathbf{Y}}_{\Re}\right) = \mathbf{F}_{N/2}\cdot\tilde{\mathbf{Y}}_{\Re} \in \mathbb{R}^{N/2},\\ \tilde{\mathbf{y}}_{\Im} &= \mathrm{IDFT}\left(\tilde{\mathbf{Y}}_{\Im}\right) = \mathbf{F}_{N/2}\cdot\tilde{\mathbf{Y}}_{\Im} \in \mathbb{R}^{N/2}.\end{aligned} \tag{12}$$

Lastly, $\tilde{\mathbf{y}}_{\Re}$ and $\tilde{\mathbf{y}}_{\Im}$, are combined as

$$\mathbf{y} = \sqrt{\kappa}\,(\tilde{\mathbf{y}}_{\Re} + j\cdot\tilde{\mathbf{y}}_{\Im}) \in \mathbb{C}^{N/2}, \tag{13}$$

where $\kappa = 2$, if only one user is considered. M-ary QAM demapping is performed on the serial symbols to obtain the output bits.

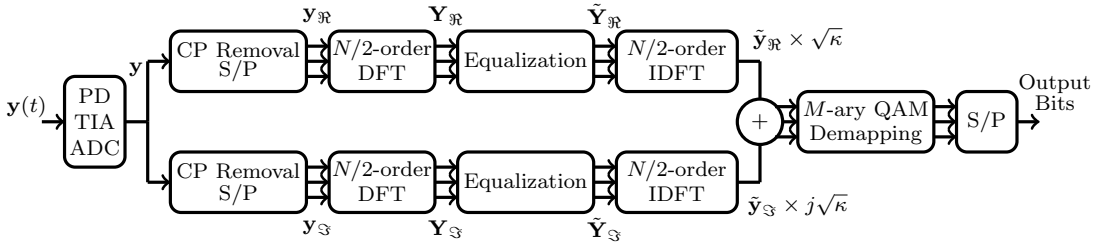

Figure 2: Block diagram of HSFO-SCFDMA receiver.

3. Statistical Characterization

Assuming uniform distribution for TD HSFO-SCFDMA signal and by adopting sufficient biasing, the average electrical and the average optical power for HSFO-SCFDMA can be calculated as

$$P_{\mathrm{elec}} = E\left[\mathbf{x}_{\beta}^2(t)\right] = E\left[\mathbf{x}^2(t)\right] + \beta_{\mathrm{dc}}^2, \tag{14}$$

and

$$P_{\mathrm{opt}} = E\left[\mathbf{x}_{\beta}(t)\right] = \beta_{\mathrm{dc}}, \tag{15}$$

respectively. The ratio of P_{elec} and P_{opt} can be expressed as

$$\alpha_{\mathrm{oe}} = \frac{P_{\mathrm{elec}}}{P_{\mathrm{opt}}}, \tag{16}$$

where α_{oe} is a measure of electrical to optical power conversion efficiency. For any value of $E_{\text{b}_{(\text{elec})}}/N_0$, the corresponding $E_{\text{b}_{(\text{opt})}}/N_0$ can be obtained using (16) and by normalizing the optical power to unity (i.e., $P_{\text{opt}} = 1$) as

$$\frac{E_{\text{b}_{(\text{opt})}}}{N_0} = \left(\frac{1}{\alpha_{\text{oe}}}\right) \frac{E_{\text{b}_{(\text{elec})}}}{N_0}. \tag{17}$$

4. Performance Evaluation

This section presents simulation and analytical results to validate and compare the performance of HSFO-SCFDMA with several other schemes. Firstly, we examine the spectral efficiencies exhibited by various modulation techniques. Secondly, we study the PAPR characteristics, where closed-form analytical expressions of PAPR for the techniques having deterministic peak values of the TD signal have been evaluated. Thereafter, we compute Monte Carlo results for BER. Subsequently, optical power penalty relative to On-Off Keying (OOK) has been analyzed. Further on, we compute the system complexities for different techniques. Lastly, we analyze quantization characteristics and electrical power efficiency considering AWGN channel.

4.1. Spectral Efficiency

Spectral efficiency is defined as the number of bits relative to modulation index times the ratio of data-carrying subchannels to the total number of available subchannels. Here, we determine the spectral efficiencies of different schemes relative to the spectral efficiencies of ACO- and DCO-OFDMA. It is recalled that ACO-OFDMA have half the spectral efficiency of DCO-OFDMA.

The spectral efficiencies for different modulation schemes are

- Both ACO- and DCO-SCFDMA have the same spectral efficiency as that of their O-OFDMA counterparts.
- DHTS-ACO-OFDM and SCO-FDM manifest same spectral efficiency as ACO-OFDMA.
- HSFO-SCFDMA exhibits the same spectral efficiency as DCO-OFDMA, therefore, it is spectrally efficient compared to ACO-SCFDMA, DHTS-ACO-OFDM, and SCO-FDM.

It can be analyzed that M^2-QAM ACO-SCFDMA and SCO-FDM would result in a same spectral efficiency as M-QAM DCO- and HSFO-SCFDMA. Moreover, M'-PAM based DHTS-ACO-OFDM and M-QAM based DCO- and HSFO-SCFDMA would result in a similar spectral efficiency, where $M' = M$.

4.2. PAPR Analysis

PAPR is the measure of variation of the TD signal about its mean. Mathematically, PAPR of an arbitrary L-order signal, z_n can be expressed as

$$\text{PAPR} = \xi \triangleq \frac{\max\limits_{0 \le n \le L-1} \left(|z_n|^2\right)}{E\left(|z_n|^2\right)}. \tag{18}$$

The PAPR of a signal can be graphically illustrated using complementary cumulative distribution function (CCDF) which is the probability that the PAPR of signal will exceed a given threshold, PAPR_ϵ, i.e., CCDF = Prob(PAPR > PAPR_ϵ).

CCDF curves are illustrated in Fig. 3 and Fig. 4 for spectral efficiencies of $\eta = 1$ bits/s/Hz and $\eta = 2$ bits/s/Hz, respectively, which reveal that HSFO-SCFDMA distinctly has the lowest PAPR. For $\eta = 1$ bits/s/Hz, HSFO-SCFDMA has a gain in PAPR of approximately 5.4 dB, 8.2 dB, 8.7 dB and 12 dB over SCO-FDM, DCO-SCFDMA, DHTS-ACO-OFDM and ACO-SCFDMA, respectively. Similarly, for $\eta = 2$ bits/s/Hz, HSFO-SCFDMA exhibits 4.8 dB, 6.4 dB, 7.5 dB and 9.4 dB lesser PAPR compared to SCO-FDM, DCO-SCFDMA, DHTS-ACO-OFDM and ACO-SCFDMA, respectively. The reduced PAPR of HSFO-SCFDMA can be translated into a power gain, as higher modulation power can be attained after the DAC.

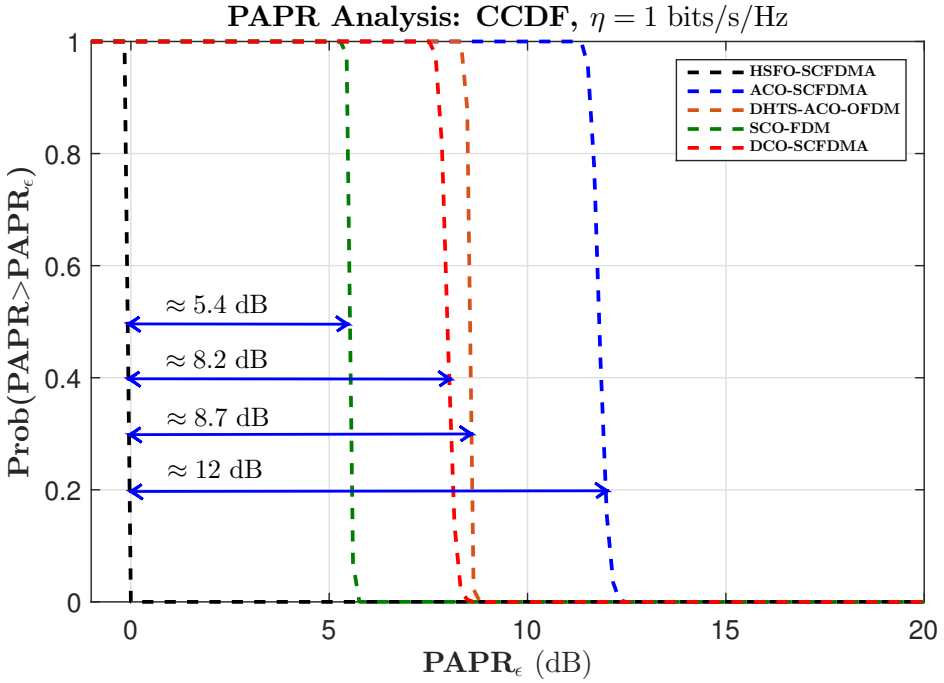

Figure 3: PAPR comparison of different modulation schemes for spectral efficiency of $\eta = 1$ bits/s/Hz.

The closed-form PAPR expressions as a function of modulation index can be readily evaluated for HSFO-SCFDMA, SCO-FDM and DHTS-ACO-OFDM, since the peak value of the TD signals are deterministic. Besides, the variance of the TD signal can be computed in a straightforward manner. The analytical expressions have been evaluated considering $M = \{4, 8, 16, 32, 64, 128, 256, 512, 1024, 2048\}$ for HSFO-SCFDMA and SCO-FDM, whereas, a generalized expression of PAPR considering M'-PAM has been obtained for DHTS-ACO-OFDM.

For HSFO-SCFDMA, the peak value, $\lambda_{\text{peak,HSFO}}$, and the variance, σ^2_{HSFO}, of the TD signal

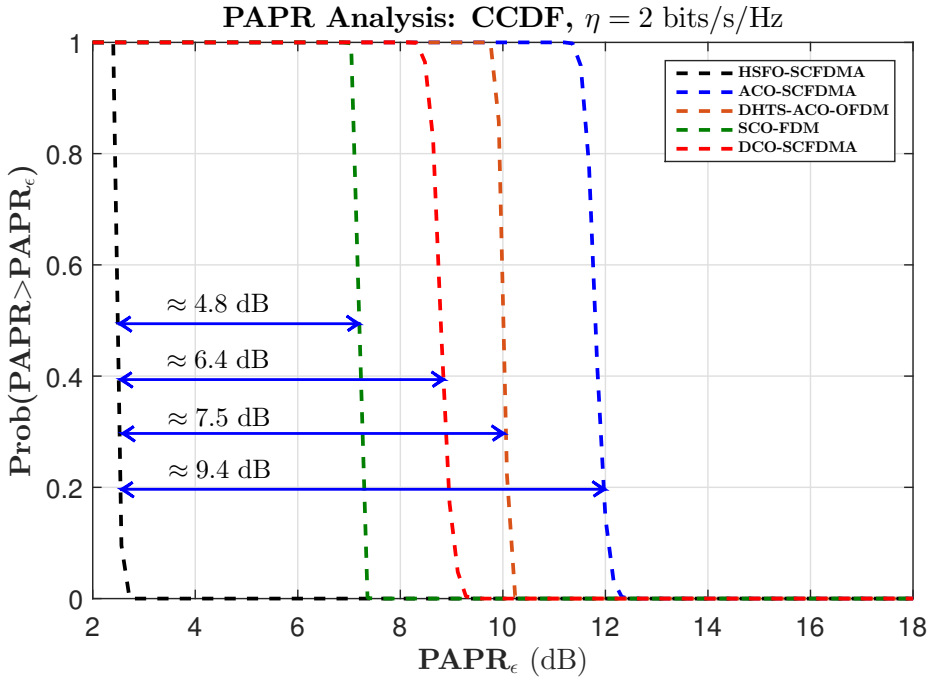

Figure 4: PAPR comparison of different modulation schemes for spectral efficiency of $\eta = 2$ bits/s/Hz.

can be given as

$$\lambda_{\text{peak,HSFO}} = \begin{cases} \frac{\sqrt{M}-1}{\sqrt{2}}, & \text{for } M = 4, 16, 64, 256, 1024 \\ \frac{\log_2(M)}{\sqrt{2}}, & \text{for } M = 8, 32 \\ \frac{2\log_2(M)-3}{\sqrt{2}}, & \text{for } M = 128 \\ \frac{2\log_2(M)+5}{\sqrt{2}}, & \text{for } M = 512 \\ \frac{4\log_2(M)+3}{\sqrt{2}}, & \text{for } M = 2048 \end{cases} \tag{19}$$

and

$$\sigma^2_{\text{HSFO}} = \begin{cases} \frac{M-1}{6}, & \text{for } M = 4, 16, 64, 256, 1024 \\ \frac{2.5M-2}{12}, & \text{for } M = 8 \\ \frac{31M-32}{192}, & \text{for } M \geq 32 \end{cases} \tag{20}$$

respectively. Thus, using (19) and (20), the closed-form expressions for the PAPR of HSFO-SCFDMA can be evaluated as $\xi_{\text{HSFO}} = \lambda^2_{\text{peak,HSFO}}/\sigma^2_{\text{HSFO}}$. For SCO-FDM, $\lambda_{\text{peak,SCO}} = (1/\sqrt{2})\lambda_{\text{peak,HSFO}}$

and $\sigma^2_{\text{SCO}} = (1/4)\sigma^2_{\text{HSFO}}$. Thus, we have

$$\xi_{\text{SCO}} = 2\xi_{\text{HSFO}}. \tag{21}$$

where, ξ_{SCO} is the PAPR exhibited by SCO-FDM. Moreover, for DHTS-ACO-OFDM, $\lambda_{\text{peak,DHTS}-\text{ACO}} \approx M' - 1$, and $\sigma^2_{\text{DHTS}-\text{ACO}} = (M'^2 - 1)/12$, with M' being the PAM modulation alphabet size. Hence, we have

$$\xi_{\text{DHTS}-\text{ACO}} = \frac{\lambda^2_{\text{peak,DHTS}-\text{ACO}}}{\sigma^2_{\text{DHTS}-\text{ACO}}} = \frac{12(M'-1)}{M'+1}, \tag{22}$$

where $\xi_{\text{DHTS}-\text{ACO}}$ is used to represent the PAPR manifested by DHTS-ACO-OFDM.

For brevity, we have skipped the evaluation of PAPR expressions for the remaining approaches. However, interested readers are referred to [28] for a comprehensive analysis of PAPR for ACO- and DCO-OFDM, which may be extended for O-SCFDMA counterparts.

4.3. Bit-Error-Rate Performance

Here, we investigate BER performance of HSFO-SCFDMA and compare it with that of ACO-SCFDMA, DHTS-ACO-OFDM, SCO-FDM, and DCO-SCFDMA considering spectral efficiencies of $\eta = \{1, 2\}$ bits/s/Hz. We consider a multipath VLC channel with a bandwidth limited LED driver combination having a 3 dB cut-off frequency of $f_{3\text{dB}} = 150$ MHz. The noise is modeled as AWGN. For DCO-SCFDMA, a bias-index of 6 dB and 10 dB is used for $\eta = 1$ bits/s/Hz and $\eta = 2$ bits/s/Hz, respectively. HSFO-SCFDMA is sufficiently biased to emphasize the augmented performance even at higher bias levels. Data-rate of $R_{\text{b}} = 200$ Mbps is considered. Thus, for $\eta = 1$ bits/s/Hz, the bandwidth (BW) of the transmitted signal is 200 MHz culminating in a prominent impact of the bandwidth limitation of the LED/LED driver combination. Whereas, for $\eta = 2$ bits/s/Hz, the bandwidth of the transmitted signal for $R_{\text{b}} = 200$ Mbps is 100 MHz, evading the bandwidth limitation of the LED/LED driver combination. As a reference, BER performance of HSFO-, DCO- (with a bias-index of 6 dB) and ACO-SCFDMA in AWGN without considering bandwidth limitation of LED/LED driver combination for $\eta = 1$ bits/s/Hz is presented. Unless otherwise specified, all results are averaged over 2000 Monte Carlo runs with number of subchannels, $N = 512$.

The results for BER versus electrical SNR per bit, $E_{\text{b}_{(\text{elec})}}/N_0$ for $\eta = 1$ bits/s/Hz and $\eta = 2$ bits/s/Hz are presented in Fig. 5 and Fig. 6, respectively, from which we can discern the following

- The electrical energy dissipation to obtain a BER of 10^{-3} for ACO-SCFDMA, DHTS-ACO-OFDM, SCO-FDM, and DCO-SCFDMA is roughly the same for $\eta = 1$ bits/s/Hz. However, ACO-SCFDMA, DHTS-ACO-OFDM, and SCO-FDM become less efficient compared to DCO-SCFDMA, as higher order modulation alphabets are required to achieve $\eta = 2$ bits/s/Hz.

- For both $\eta = \{1, 2\}$ bits/s/Hz, HSFO-SCFDMA signifies a superior performance compared to other alternatives. It may be noted that for $\eta = 1$ bits/s/Hz, to achieve a BER of 10^{-3}, HSFO-SCFDMA delivers an electrical power gain of approximately 2 dB over ACO-SCFDMA

and DHTS-ACO-OFDM, and around 3 dB over DCO-SCFDMA and SCO-FDM. For $\eta = 2$ bits/s/Hz at BER of 10^{-3}, a gain of almost 5 dB over DCO-SCFDMA, and nearly 6 dB over ACO-SCFDMA, DHTS-ACO-OFDM, and SCO-FDM can be observed for HSFO-SCFDMA.

- Comparing HSFO-SCFDMA with DCO-SCFDMA, the gain in BER is correlated to the difference in bias required to achieve non-negativity. Whereas, for the remaining schemes, the gain is observed because lower order constellations are needed to achieve a given spectral efficiency for HSFO-SCFDMA, while higher order modulation alphabets are required for other approaches.

- If $R_{\mathrm{b}} = 200$ Mbps is considered for $\eta = 2$ bits/s/Hz, the BER performance of all the schemes is close to their performance in AWGN because the dispersive impact of the VLC multipath channel and the bandwidth limitation of the LED/LED driver combination is averted due to low bandwidth of the transmitted signal.

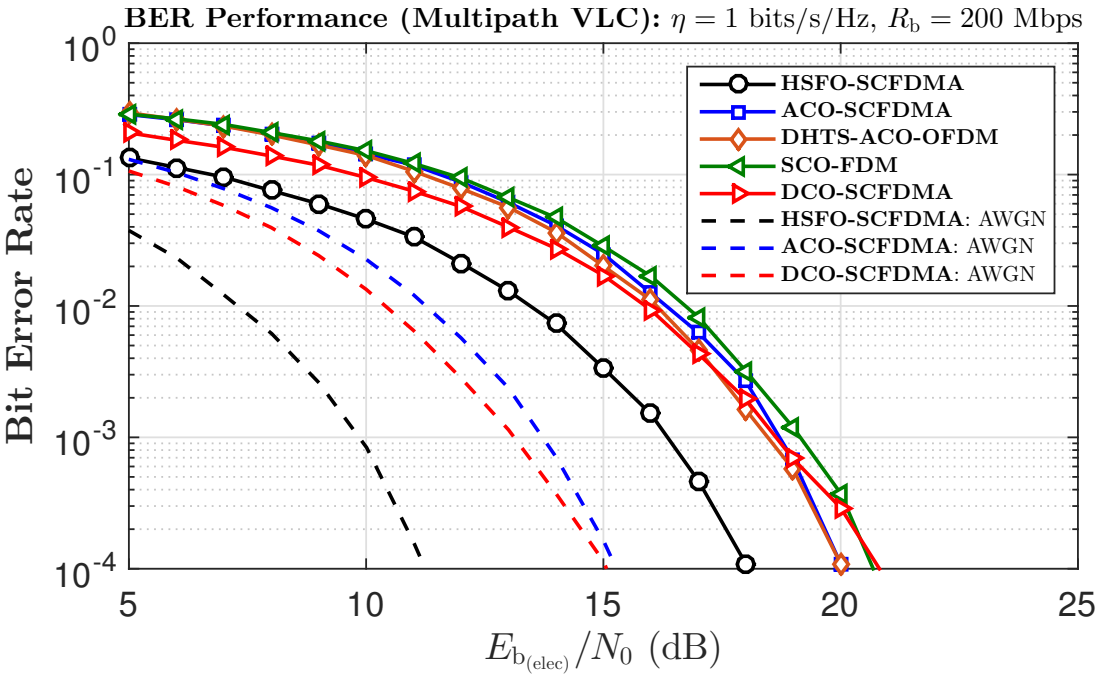

Figure 5: BER performance as a function of $E_{\mathrm{b}_{(\mathrm{elec})}}/N_0$ in multipath VLC channel considering a spectral efficiency of $\eta = 1$ bits/s/Hz. $R_{\mathrm{b}} = 200$ Mbps and $f_{3\mathrm{dB}} = 150$ MHz are considered. The bias-index for DCO-SCFDMA is 6 dB, while HSFO-SCFDMA is sufficiently biased. The dashed curves represent the performance of different modulation schemes in an AWGN channel.

4.4. Optical Power Penalty

In this section, the optical power penalty for different modulation approaches incurred due to the bandwidth limitation of the LED/LED driver combination and the VLC channel has been

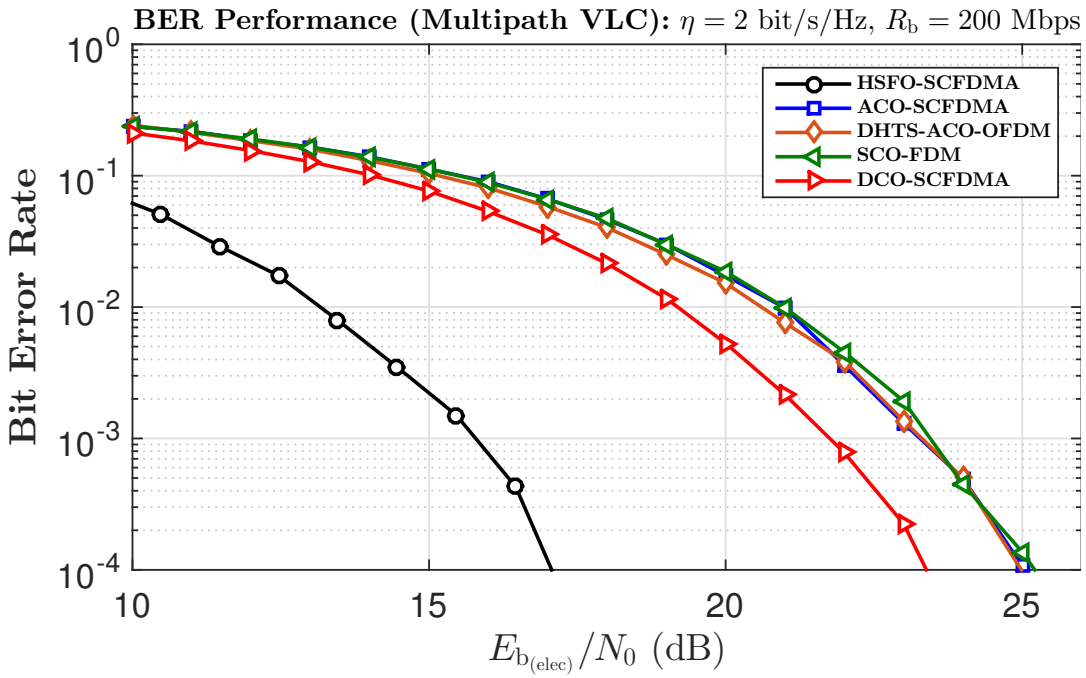

Figure 6: BER performance as a function of $E_{\mathrm{b}_{(\mathrm{elec})}}/N_0$ in multipath VLC channel considering a spectral efficiency of $\eta = 2$ bits/s/Hz. $R_{\mathrm{b}} = 200$ Mbps and $f_{3\mathrm{dB}} = 150$ MHz are considered. The bias-index of DCO-SCFDMA is 10 dB, while HSFO-SCFDMA is sufficiently biased.

analyzed. For a given BER, P_{b}, the optical power penalty is obtained by normalizing the required optical power by the average optical power required for OOK, $E^{\mathrm{OOK}}_{\mathrm{b}_{(\mathrm{opt})}}/N_0$, in an AWGN channel with no bandwidth limitation. $E^{\mathrm{OOK}}_{\mathrm{b}_{(\mathrm{opt})}}/N_0$ to obtain P_{b} can be given as

$$E^{\mathrm{OOK}}_{\mathrm{b}_{(\mathrm{opt})}}/N_0 = \mathrm{erfc}^{-2}\left(2P_{\mathrm{b}}\right), \tag{23}$$

where $\mathrm{erfc}(\phi)$ is the complementary error function expressed as $\mathrm{erfc}(\phi) = 1 - 2/\sqrt{\pi}\int_0^{\phi}\exp(-t^2)\mathrm{d}t$. The results are achieved by setting $P_{\mathrm{b}} = 10^{-3}$ and varying the ratio of the data-rate to the 3 dB optical cut-off frequency, i.e., $R_{\mathrm{b}}/f_{3\mathrm{dB}}$. Multipath VLC channel and spectral efficiency of $\eta = 2$ bits/s/Hz is recognized, and the result is illustrated in Fig. 7, from which following observations can be made

- DCO-SCFDMA experiences the largest optical power penalty compared to other alternatives because of the bias.
- The optical power penalty for SCO-FDM is somewhat larger compared to ACO-SCFDMA and DHTS-ACO-OFDM.
- DHTS-ACO-OFDM undergoes the same optical power penalty as that of ACO-SCFDMA for

$R_{\rm b}/f_{\rm 3dB} \leq 1.90$. However, for $R_{\rm b}/f_{\rm 3dB} > 1.90$, the performance of DHTS-ACO-OFDM is peculiar, because the optical power penalty increases substantially if high data-rates are used.

- HSFO-SCFDMA exhibits superior performance for all the values of $R_{\rm b}/f_{\rm 3dB}$, since, it suffers the least optical power penalty. For $R_{\rm b}/f_{\rm 3dB} \leq 1.90$, DCO-SCFDMA and SCO-FDM, respectively, perform approximately 6 dB and 3.5 dB worse compared to HSFO-SCFDMA, whereas, ACO-SCFDMA and DHTS-ACO-OFDM are penalized 3 dB more than HSFO-SCFDMA.

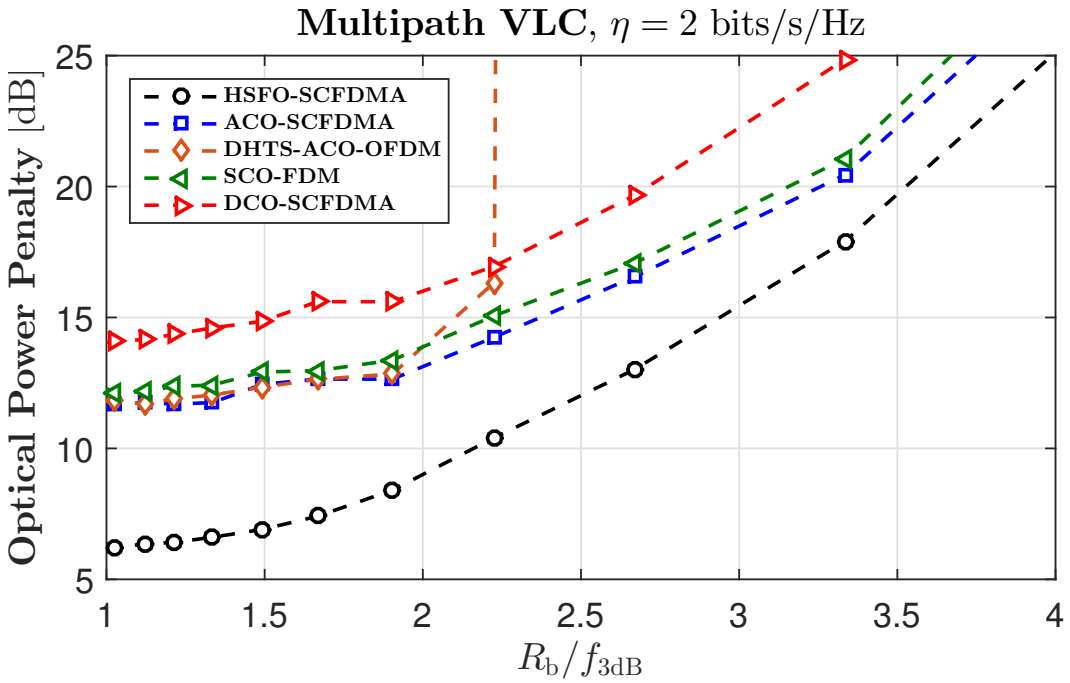

Figure 7: Optical power penalty as a function of $R_{\rm b}/f_{\rm 3dB}$ in multipath VLC channel. Spectral efficiency of $\eta = 2$ bits/s/Hz and $f_{\rm 3dB} = 150$ MHz are considered. The bias-index for DCO-SCFDMA is 10 dB, while HSFO-SCFDMA is sufficiently biased.

4.5. Complexity Analysis

In this section, we analyze the computational complexity incurred by various modulation schemes. The complexity analysis in terms of probability of convergence, theoretical run-time boundaries etc. can be cumbersome. Hence, system complexity is calculated in terms of a total number of required arithmetic operations at the transceiver. We consider that a block of N data symbols is taken as an input by the transceivers. We further assume that DFT/IDFT order is also equal to N. For an efficient implementation, we consider that DFT and IDFT are implemented utilizing fast Fourier transform (FFT) and inverse FFT (IFFT) algorithms, respectively. Thus, an N-order FFT/IFFT would approximately require $4N\log_2(N)$ arithmetic operations [29]. In both O-OFDMA and O-SCFDMA systems, the complexity is due to the FFT/IFFT and equalization. Due to the diagonal

nature of $\mathbf{\Lambda}$, equalization can be realized in $\mathcal{O}(N)$ operations [30], thus, in the sequel, we only consider the complexity incurred due to FFT/IFFT. The complexities of different modulation approaches are

- For HSFO-SCFDMA, $N/2$-order FFT and N-order IFFT are performed at the transmitter, whereas, at the receiver, two $N/2$-order FFT and two $N/2$-order IFFT are required.
- For ACO-SCFDMA, $N/4$-order FFT and N-order IFFT are required at the transmitter, whereas, at the receiver, FFT/IFFT are inveresed, i.e., N-order FFT and $N/4$-order IFFT are needed.
- In DHTS-ACO-OFDM, real constellations along with DHT are used. N-order DHT approximately requires $2N\log_2(N)$ arithmetic operations [31]. At the transmitter, $N/2$-order DHT and N-order IDHT are performed. Additionally, at the receiver, N-order DHT and $N/2$-order IDHT are taken.
- For SCO-FDM, an optimized variant with an efficient equalization process has been implemented. In our implementation, at the transmitter, $N/4$-order FFT and N-order IFFT operations are required, whereas, at the receiver, four $N/4$-order FFT and one $N/4$-order IFFT are needed.
- For DCO-SCFDMA, $N/2-1$-order FFT and N-order IFFT are required at the transmitter, while, N-order FFT and $N/2-1$-order IFFT are taken at the receiver.

Overall system complexities for various modulation schemes are compiled in Table 1 and plotted as a function of input block size, N scaled by the spectral efficiency, η, in Fig. 8. Scaling is performed to ensure a fair comparison, e.g., to achieve a given data-rate, if HSFO-SCFDMA requires an input block size of N, ACO-SCFDMA (or a scheme with similar spectral efficiency) would require a block size of $2N$. Fig. 8 reveals that DCO-SCFDMA and DHTS-ACO-OFDM manifests the least computational complexity, whereas, HSFO-SCFDMA is less complex compared to ACO-SCFDMA and SCO-FDM. We highlight that even though the computational complexity of HSFO-SCFDMA is marginally higher compared to DCO-SCFDMA and DHTS-ACO-OFDM, yet, HSFO-SCFDMA demonstrates superior performance compared to DCO-SCFDMA and DHTS-ACO-OFDM in other performance parameters.

4.6. Quantization Characteristics

In this subsection, we investigate the impact of quantization by evaluating the effective number of bits required to achieve a target BER. Following [32], the required electrical SNR per bit in an AWGN channel, $E^{\text{req}}_{\text{b}_{(\text{elec})}}/N_0$, for the target BER is evaluated, using which the effective number of bits are calculated. A target BER of 10^{-3} and uniform quantization is considered. The quantization noise is modeled as an additive, uniformly distributed white noise [32].

As λ_{peak}, for HSFO-SCFDMA, DHTS-ACO-OFDM, and SCO-FDM are deterministic, calculating the effective number of bits is rather straightforward. Whereas, for remaining approaches,

Table 1: Computational complexity of different modulation techniques.

Modulation Scheme	Complexity
HSFO-SCFDMA	$4N\log_2(N) + 10N\log_2(N/2)$
ACO-SCFDMA	$8N\log_2(N) + 2N\log_2(N/4)$
DHTS-ACO-OFDM	$4N\log_2(N) + 2N\log_2(N/2)$
SCO-FDM	$4N\log_2(N) + 6N\log_2(N/4)$
DCO-SCFDMA	$8N\log_2(N) + (4N-8)\log_2(N/2-1)$

Monte Carlo averaging is needed to obtain an estimate of λ_{peak}. The TD signals of HSFO-SCFDMA and SCO-FDM manifest distinct number of levels as a function of the modulation index, M. This feature simplifies the calculation of the required effective number of bits for the transmitter of HSFO-SCFDMA and SCO-FDM. Both HSFO-SCFDMA and SCO-FDM would require the same effective number of bits no matter what the $E^{\text{req}}_{\text{b}_{(\text{elec})}}/N_0$ is. However, the received signals for HSFO-SCFDMA and SCO-FDM are analog and suffer from the noise, so, the signals no longer manifest discrete levels. Thus, by following [32], the effective number of bits for HSFO-SCFDMA and SCO-FDM, at the receiver, are calculated based on $E^{\text{req}}_{\text{b}_{(\text{elec})}}/N_0$. Consequently, for HSFO-SCFDMA and SCO-FDM, the effective number of bits required at the receiver differ from the number of bits required at the transmitter. For the remaining techniques, same effective number of bits are considered at both the transmitter and the receiver [32].

Table 2 presents the analytical formulae to compute the effective number of bits at the transmitter and receiver to achieve a BER of 10^{-3}. Graphical illustrations have been provided in Fig. 9 and Fig. 10 which show that for a given spectral efficiency, the effective number of bits required by the transmitter or the receiver of HSFO-SCFDMA are less compared to other counterparts.

From the results, we can perceive that the bit resolution requirement of both the ADC and DAC can be relaxed if HSFO-SCFDMA is adopted, thus, the overall cost of the system can be reduced.

4.7. Power Efficiency

Fig. 11 depicts how $\langle E_{\text{b}_{(\text{elec})}}/N_0\rangle$ (the required $E_{\text{b}_{(\text{elec})}}/N_0$ to achieve a BER of 10^{-3}) in an AWGN channel varies with the spectral efficiency, η. For HSFO- and DCO-SCFDMA, spectral efficiencies, η between $[1, 6.5]$ bits/s/Hz are considered, whereas, for ACO-SCFDMA, SCO-FDM, the spectral efficiencies between $[0.5, 3.25]$ bits/s/Hz are taken into account. Note that, $\eta = 3.25$ bits/s/Hz (for ACO-SCFDMA and SCO-FDM) corresponds to 8192-QAM, hence, evaluating the power efficiencies for $\eta > 3.25$ bits/s/Hz might not be meaningful. For DHTS-ACO-OFDM, spectral efficiencies between $[0.5, 2.5]$ bits/s/Hz are investigated. Besides, for DCO-SCFDMA, the results are obtained by recognizing 6 dB bias for $\eta = 1$ bits/s/Hz, 7.5 dB for $\eta = 1.5$ bits/s/Hz and a bias of 10 dB for $\eta \geq 2$ bits/s/Hz.

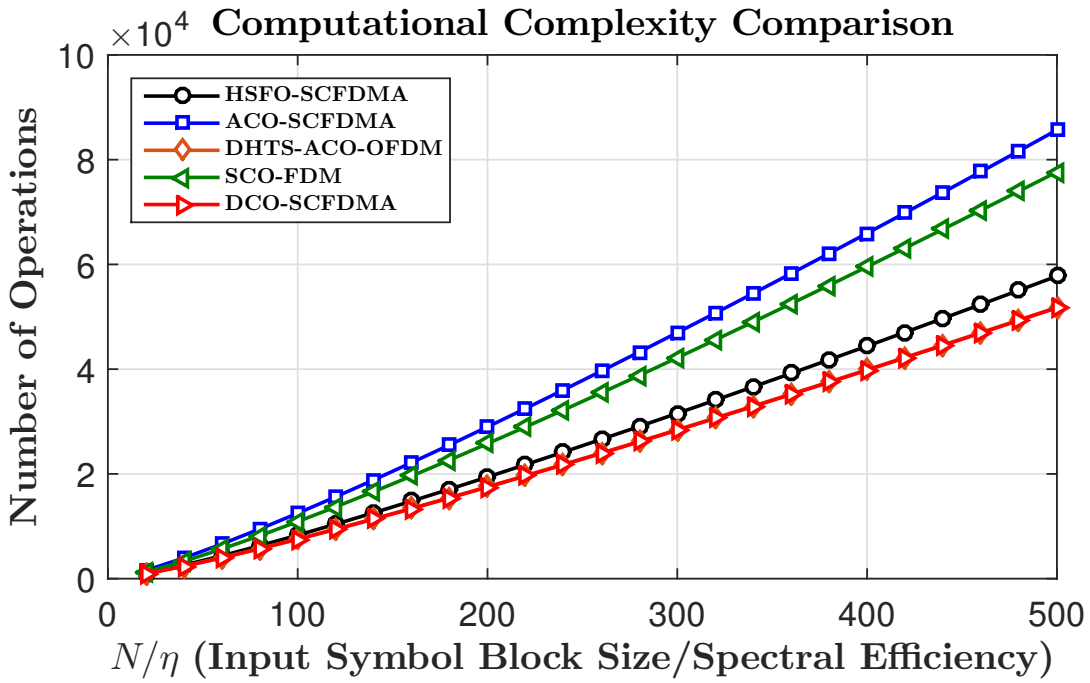

Figure 8: Complexity comparison of different modulation schemes. The block size N is normaized with the spectral efficiency, η to ensure same data-rate.

It has been established that HSFO-SCFDMA demonstrates a superior performance compared to other alternatives, e.g., for $\eta = 2$ bits/s/Hz, it attains a power efficiency gain of almost 5.2 dB over DCO-SCFDMA, and approximately 8 dB over ACO-SCFDMA, DHTS-ACO-OFDM and SCO-FDM. Moreover, for low spectral efficiencies, DCO-SCFDMA signifies the same power efficiency as that of ACO-SCFDMA, DHTS-ACO-OFDM, and SCO-FDM. However, for higher spectral efficiencies, DCO-SCFDMA becomes more power efficient compared to ACO-SCFDMA, DHTS-ACO-OFDM and SCO-FDM. Similar trends can be expected if optical power efficiency is computed.

5. Multiple Access

In this section, we explain the MA capability of HSFO-SCFDMA. LED lighting source consisting of LED array, K users and N subchannels are considered. All the users employ same M-ary QAM constellations. Each user has the feasibility to modulate $N/2^K$ subchannels. For kth user, the TD symbol vector is given as $\mathbf{s}_k \in \mathbb{C}^{N/2^K}$, and the corresponding DFT-precoded FD symbol vector is obtained by using $N/2^K$-order DFT as

$$\mathbf{S}_k = \mathrm{DFT}\left(\mathbf{s}_k\right) = \mathbf{F}_{N/2^K} \cdot \mathbf{s}_k \in \mathbb{C}^{N/2^K}. \tag{24}$$

Table 2: Effective number of bits required at the transmitter and the receiver for different modulation schemes. $\lfloor\cdot\rfloor$ represents ceiling operation to nearest integer. γ_{HSFO} and γ_{SCO}, respectively, are the number of distinct levels of TD signal for HSFO-SCFDMA and SCO-FDM. α is the bias coefficient for DCO-SCFDMA. σ^2 represents the transmitted signal power for the respective modulation scheme. λ_{peak} for ACO-SCFDMA has been evaluated after clipping.

TRANSMITTER	
Modulation Scheme	Effective Number of Bits
HSFO-SCFDMA	$\lfloor \log_2[\gamma_{\text{HSFO}}] \rfloor$
ACO-SCFDMA	$\left\lfloor 0.5 \log_2 \left[\frac{\lambda_{\text{peak}}^2}{6\sigma^2} \frac{E_{\text{b}_{(\text{elec})}}^{\text{req}}}{N_0} \right] \right\rfloor$
DHTS-ACO-OFDM	$\left\lfloor 0.5 \log_2 \left[\frac{2\left(M'-1\right)}{(M'+1)} \frac{E_{\text{b}_{(\text{elec})}}^{\text{req}}}{N_0} \right] \right\rfloor$
SCO-FDM	$\lfloor \log_2[\gamma_{\text{SCO}}] \rfloor$
DCO-SCFDMA	$\left\lfloor 0.5 \log_2 \left[\frac{4\lambda_{\text{peak}}^2 + \left(\lambda_{\text{peak}} + \alpha\sigma\right)^2}{12\sigma^2} \frac{E_{\text{b}_{(\text{elec})}}^{\text{req}}}{N_0} \right] \right\rfloor$
RECEIVER	
Modulation Scheme	Effective Number of Bits
HSFO-SCFDMA	$\left\lfloor 0.5 \log_2 \left[\frac{\lambda_{\text{peak}}^2}{3\sigma^2} \frac{E_{\text{b}_{(\text{elec})}}^{\text{req}}}{N_0} \right] \right\rfloor$
SCO-FDM	$\left\lfloor 0.5 \log_2 \left[\frac{\lambda_{\text{peak}}^2}{12\sigma^2} \frac{E_{\text{b}_{(\text{elec})}}^{\text{req}}}{N_0} \right] \right\rfloor$

From (24), it is inferred that for K users $N/2^K$-order DFT-precoding would be required. Subchannel mapping is performed such that each user is allocated unique subchannels. For kth user, the FD precoded symbols from $\mathbf{S}_k$ are mapped to $\tilde{\mathbf{S}}_k \in \mathbb{C}^N$ on indexes $2(k-1) : 2^K - 1 : N$, with $2^K - 1$ zeros padded between the two adjacent modulated subchannels. The TD counterparts of $\tilde{\mathbf{S}}_k \ \forall \ k = 1, \cdots, K$ are transmitted using different LEDs in the array as depicted in Fig. 12 for a system with $K = 2$. N-order IDFT is applied to $\tilde{\mathbf{S}}_k$ to obtain

$$\tilde{\mathbf{s}}_k = \text{IDFT}\left(\tilde{\mathbf{S}}_k\right) = \mathbf{F}_N^{\text{H}} \cdot \tilde{\mathbf{S}}_k \in \mathbb{C}^N. \tag{25}$$

$\tilde{\mathbf{s}}_k$ exhibit a half-wave symmetry, from which, the real and imaginary sub-blocks for kth user can be obtained as

$$\mathbf{x}_{k,\Re} = \Re\left[\tilde{\text{s}}_k^{(n)}\right], \ \mathbf{x}_{k,\Im} = \Im\left[\tilde{\text{s}}_k^{(n+N/2)}\right], \tag{26}$$

$\forall \ n = 0, 1, \cdots, N/2-1$, respectively, where $\{\mathbf{x}_{k,\Re}, \mathbf{x}_{k,\Im}\} \in \mathbb{R}^{N/2} \ \forall \ k = 1, \cdots, K$. The IM consistent signal $[\mathbf{x}_{k,\Re} \ \mathbf{x}_{k,\Im}]^{\text{T}}$ is transmitted through LEDs.

The receiver is exactly the same as presented in Fig. 2. At the receiver, signal consisting of the sum of all the users is obtained. After processing, the received symbols for different users are distinguished by choosing the correct subchannels. Note that, the received symbol vector would always be $N/2$-order, from which the allocated subchannels for kth user can be obtained as

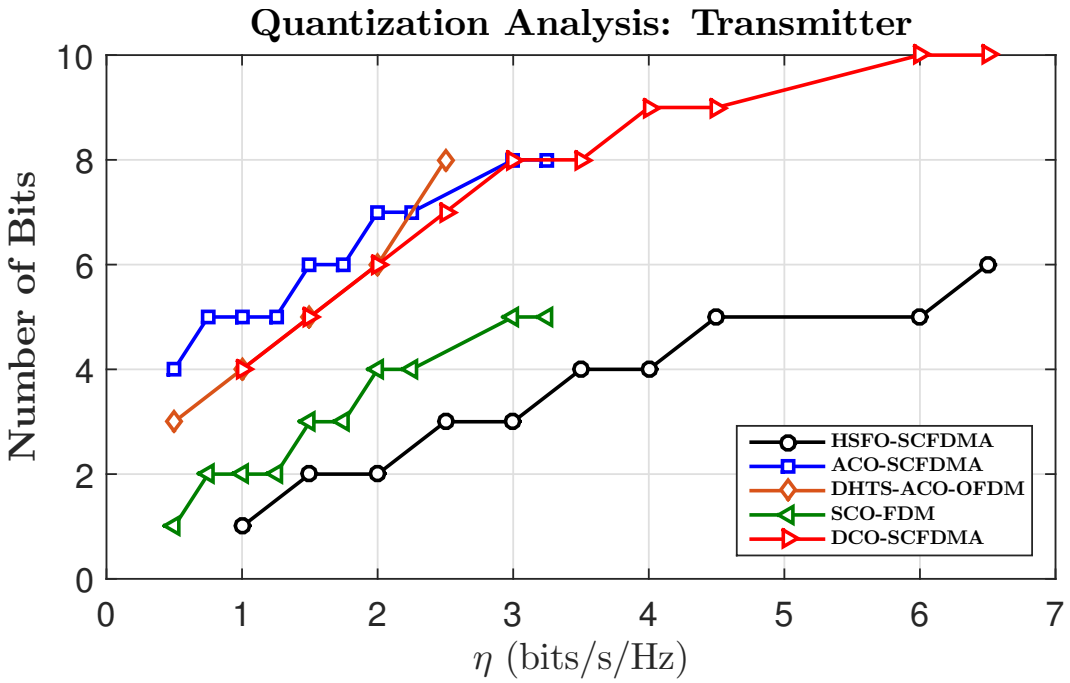

Figure 9: Effective number of bits required for quantization by the transmitter for different modulation schemes.

$(k-1):K:N/2$. Moreover, κ also depends on the number of users in the system, thus, if K users are considered, the value of κ would be equal to 2^K.

From the presented analysis, it can be ascertained that HSFO-SCFDMA can be employed in a VLC down-link scenario, for which each LED in the array transmits the data/information for a different user.

6. Conclusions

In this article, we study O-SCFDMA as an alternate to O-OFDMA. From the study of the proposed HSFO-SCFDMA, following conclusions can be drawn:

1. HSFO-SCFDMA possesses same spectral efficiency as DCO-SCFDMA, whereas, the spectral efficiencies of ACO-SCFDMA, DHTS-ACO-FDM and SCO-FDM are half of HSFO-SCFDMA. Accordingly, same spectral efficiency is obtained by employing higher modulation alphabets for ACO-SCFDMA, DHTS-ACO-OFDM and SCO-FDM.
2. HSFO-SCFMA manifests significantly reduced PAPR compared to the other counterparts which results in power efficiency through a limited bit resolution DAC, and less sensitivity to any non-linear impairments. Moreover, the power efficiency could be vital to enhance the battery life if considered for user terminal.

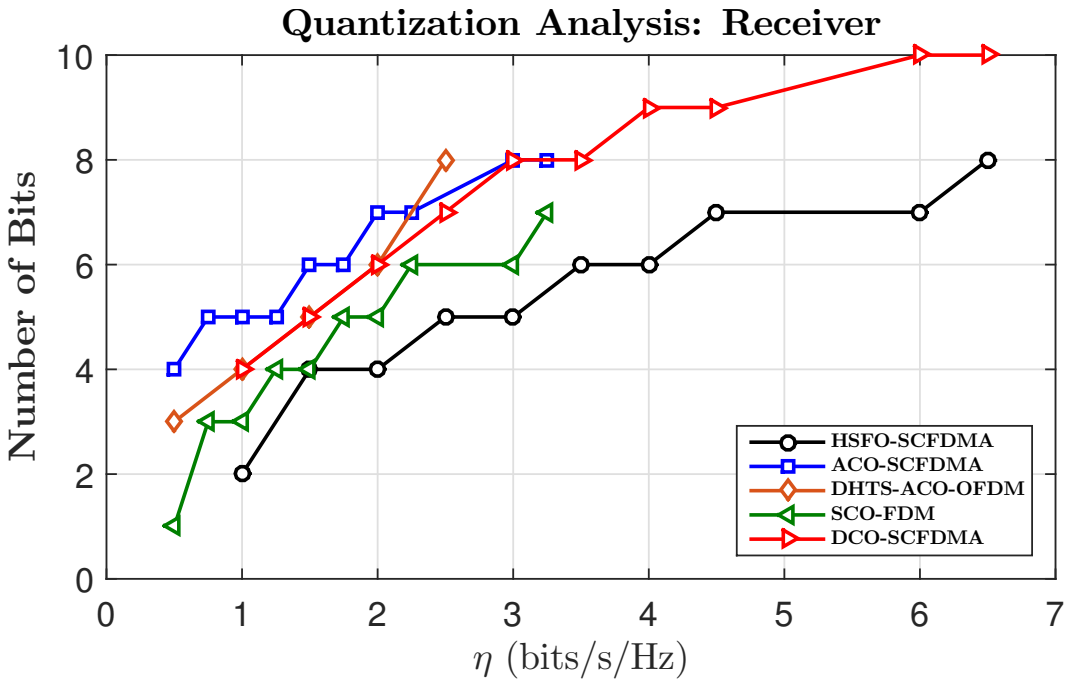

Figure 10: Effective number of bits required for quantization by the receiver for different modulation schemes.

3. As expected from 1) and 2), it is determined that the bit resolution requirement of both DAC and ADC for HSFO-SCFDMA can be relaxed, consequently, the overall cost of the system can be reduced.
4. HSFO-SCFDMA exhibits enhanced BER performance compared to other alternatives considering multipath VLC channel and bandwidth limitation of LED/LED driver combination.
5. HSFO-SCFDMA undergoes the least optical power penalty compared to other alternatives. Besides, HSFO-SCFDMA also achieves the lowest optical power penalty floor compared to other counterparts.
6. HSFO-SCFDMA is less complex than ACO-SCFDMA and SCO-FDM. However, it is more complex compared to DCO-SCFDMA and DHTS-ACO-OFDM, but, surpasses them in other performance parameters.
7. HSFO-SCFDMA is the most power efficient approach in terms of electrical power dissipation to obtain a given BER of 10^{-3}.

References

[1] S. Dimitrov, S. Sinanovic, and H. Hass. Clipping noise in OFDM-based optical wireless communication systems. *IEEE Trans. Commun.*, 60(4):1072–1081, 2012.

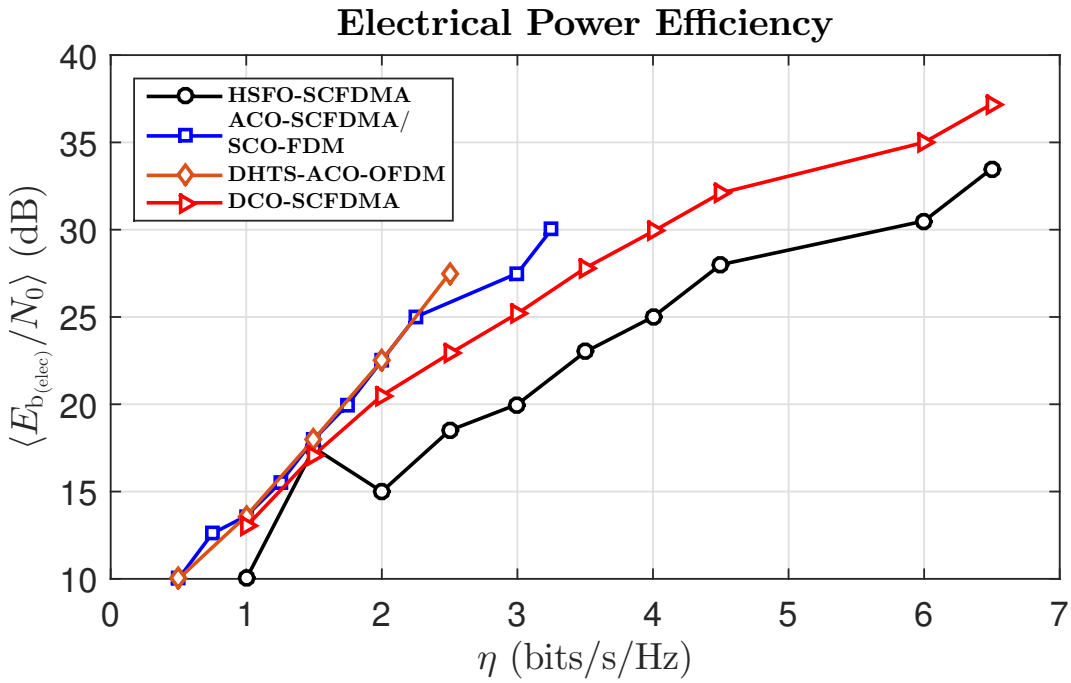

Figure 11: Analysis of electrical power efficiency of different modulation techniques. The average $E_{b_{(elec)}}/N_0$ for a BER of 10^{-3} represented as $\langle E_{b_{(elec)}}/N_0\rangle$ has been evaluated for different spectral efficiencies, η.

[2] Carruthers J. B. and J. M. Kahn. Multiple-subcarrier modulation for nondirected wireless infrared communication. *IEEE J. Sel. Areas Commun.*, 14(3):538–546, 1996.

[3] J. Armstrong and A. J. Lower. Power efficient optical OFDM. *Electron. Lett*, 42(6):370–372, 2006.

[4] J. Armstrong. OFDM for optical communications. *J. Lightw. Tech.*, 27(3):189–204, 2009.

[5] H. Elgala, R. Mesleh, and H. Haas. Indoor optical wireless communication: potential and state-of-the-art. *IEEE Commun. Mag.*, 49(9), 2011.

[6] N. Fernando, Y. Hong, and E. Viterbo. Flip-OFDM for unipolar communication systems. *IEEE Trans. Commun.*, 60(12):3726–3733, 2012.

[7] F. Barrami, Y. Le Guennec, E. Novakov, J.-M. Duchamp, and P. Busson. A novel FFT/IFFT size efficient technique to generate real time optical OFDM signals compatible with IM/DD systems. *Euro. Microw. Conf.*, pages 1247–1250, 2013.

[8] A. W. Azim, Y. Le Guennec, and G. Maury. Decision-directed iterative methods for PAPR reduction in optical wireless OFDM systems. *Opt. Commun.*, 389:318–330, 2017.

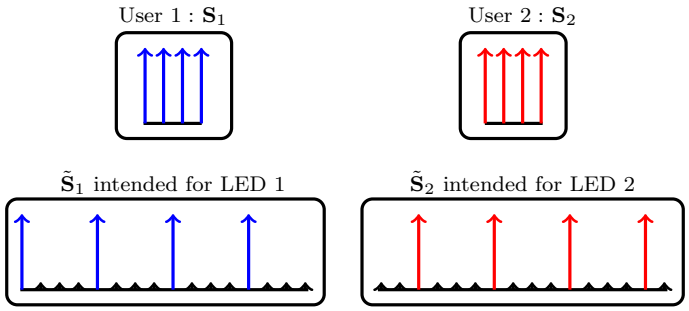

Figure 12: Illustration of subchannel mapping for two different users.

[9] W. O. Popoola, Z. Ghassemlooy, and B. G. Stewart. Pilot-assisted PAPR reduction technique for optical OFDM communication systems. *J. of Lightw. Tech.*, 32(7):1374–1382, 2014.

[10] C. R. Berger, Y. Benlachtar, R. I. Killey, and P. A. Milder. Theoretical and experimental evaluation of clipping and quantization noise for optical OFDM. *Opt. Express*, 19(18):17713–17728, 2011.

[11] T. Mao, Z. Wang, Q. Wang, and L. Dai. Ellipse-based DCO-OFDM for visible light communications. *Opt. Commun.*, 360:1–6, 2016.

[12] H. Zhang, Y. Yuan, and W. Xu. Papr reduction for DCO-OFDM visible light communications via semidefinite relaxation. *IEEE Photo.Tech. Letter*, 26(17):1718–1721, 2014.

[13] H. Marshoud, S. Muhaidat, P. C. Sofotasios, S. Hussain, M. A. Imran, and B. S. Sharif. Optical non-orthogonal multiple access for visible light communication. *arXiv preprint arXiv:1704.07621*, 2017.

[14] D. Tsonev, S. Videv, and H. Haas. Light fidelity (Li-Fi): towards all-optical networking. *SPIE OPTO*, pages 900702–900702, 2013.

[15] R. Mesleh, H. Elgala, and H. Haas. LED nonlinearity mitigation techniques in optical wireless OFDM communication systems. *J. Opt. Commun. and Network.*, 4(11):865–875, 2012.

[16] C. Wu, H. Zhang, and W. Xu. On visible light communication using LED array with DFT-spread OFDM. *IEEE ICC*, pages 3325–3330, 2014.

[17] O. Saied, Z. Ghassemlooy, R. C. Kizilirmak, X. Dai, C. Ribeiro, M. Zhang, and S. Rajbhandari. Single carrier optical FDM in visible light communication. *IEEE CSNDSP*, pages 1–5, 2016.

[18] J. Zhou and Y. Qiao. Low-PAPR asymmetrically clipped optical OFDM for intensity-modulation/direct-detection systems. *IEEE Photon. J.*, 7(3):1–8, 2015.

[19] J. Zhou and Y. Qiao. Low-peak-to-average power ratio and low-complexity asymmetrically clipped optical orthogonal frequency-division multiplexing uplink transmission scheme for long-reach passive optical network. *Optics letters*, 40(17):4034–4037, 2015.

[20] Y. S. Cho, J. Kim, W. Y. Yang, and C. G. Kang. *MIMO-OFDM wireless communications with MATLAB*. John Wiley & Sons, 2010.

[21] N. Wu and Y.l Bar-Ness. A novel power-efficient scheme asymmetrically and symmetrically clipping optical (ASCO)-OFDM for IM/DD optical systems. *EURASIP J. Adv. Sig. Process.*, 2015(1):3, 2015.

[22] A. Weiss, A. Yeredor, and M. Shtaif. Iterative symbol recovery for power-efficient dc-biased optical ofdm systems. *J. Lightw. Tech.*, 34(9):2331–2338, 2016.

[23] H. Elgala, R. Mesleh, and H. Haas. Practical considerations for indoor wireless optical system implementation using ofdm. *IEEE ConTEL*, pages 25–29, 2009.

[24] M. Wolf, S. A. Cheema, M. A. Khalighi, and S. Long. Transmission schemes for visible light communications in multipath environments. *Intl. Conf. on Transparent Opt. Networks*, pages 1–7, 2015.

[25] F. R. Gfeller and U. Bapst. Wireless in-house data communication via diffuse infrared radiation. *Proceedings of the IEEE*, 67(11):1474–1486, 1979.

[26] K. Lee, H. Park, and J. R. Barry. Indoor channel characteristics for visible light communications. *IEEE Commun. Lett.*, 15(2):217–219, 2011.

[27] A. Nuwanpriya, S.-W. Ho, J. A. Zhang, A. J. Grant, and L. Luo. PAM-SCFDE for optical wireless communications. *Journal of Lightwave Technology*, 33(14):2938–2949, 2015.

[28] J. Wang, Y. Xu, X. Ling, R. Zhang, Z. Ding, and C. Zhao. PAPR analysis for OFDM visible light communication. *Opt. Express*, 24(24):27457–27474, 2016.

[29] S. G. Johnson and M. Frigo. A modified split-radix FFT with fewer arithmetic operations. *IEEE Trans. Sig. Process.*, 55(1):111–119, 2007.

[30] P. Schniter. Low-complexity equalization of OFDM in doubly selective channels. *IEEE Trans. Sig. Process.*, 52(4):1002–1011, 2004.

[31] J. Zhou, Y. Qiao, Z. Cai, and Y. Ji. An improved scheme for flip-OFDM based on Hartley transform in short-range IM/DD systems. *Opt. Express*, 22(17):20748–20756, 2014.

[32] J. K. Perin, M. Sharif, and J. M. Kahn. Modulation schemes for single-laser 100 Gb/s links: Multicarrier. *J. Lightw. Techn.*, 33(24):5122–5132, 2015.